

A 3D Statistical Shape Model Of The Pelvic Bone For Segmentation

Hans Lamecker^a, Martin Seebaß^b, Hans-Christian Hege^a, Peter Deuffhard^a

^aZuse Institute, Takustr. 7, 14195 Berlin, Germany;

^bIndeed Visual Concepts GmbH, Ihnestr. 23, 14195 Berlin, Germany

ABSTRACT

Statistical models of shape are a promising approach for robust and automatic segmentation of medical image data. This work describes the construction of a statistical shape model of the pelvic bone. An interactive approach is proposed for solving the correspondence problem which is able to handle shapes of arbitrary topology, suitable for the genus 3 surface of the pelvic bone. Moreover it allows to specify corresponding anatomical features as boundary constraints to the matching process. The model's capability for segmentation was tested on a set of 23 CT data sets. Quantitative results will be presented, showing that the model is well suited for segmentation purposes.

Keywords: statistical shape models, 3d correspondence problem, model-based segmentation, pelvic bone

1. INTRODUCTION

1.1. Motivation

Hyperthermia is a promising approach in cancer therapy. The method is based on heating up affected tissue compartments to temperatures above 42 degree Celsius without damaging surrounding tissue compartments. In regional hyperthermia tumors in the pelvic region are heated using radio waves. Treatment planning consists of simulating and optimizing the temperature distribution in the patient with the aim of computing optimal antenna parameters. This requires the generation of individual patient models from 3D image data.

Within the setting of a hybrid system (applicator plus MR tomograph, see figure 1, left) MRT images showing the actual patient position in the applicator can be used for therapy planning. This reduces inaccuracies introduced by the former approach where the planning was performed on the basis of CT data. However, the segmentation of MRT images is a quite difficult task. An automatic pre-segmentation via thresholding is not possible because there is no specific range of gray values for bone. In some regions the contour of the pelvic bone is hard to detect (see figure 1, right). Currently the manual segmentation of the pelvic bone is the most time consuming part of the whole planning procedure.

We propose the use of a statistical shape model for semi-automatic segmentation of the pelvic bone, based on its representation as a surface mesh. From a set of training data, the typical shape of the pelvic bone and the most significant modes of variation are determined (training phase, section 2). This shape information can be subsequently used for the segmentation of new image data (segmentation phase, section 3), restricting the result to a legal shape instance of the object to be segmented. This yields inherent robustness needed for automizing the task of segmentation.

The model's capability for segmentation was tested on a set of 23 CT data sets. Ultimately the model shall be used for the segmentation of MRT data. The adaption of the shape model to MRT data however is rather difficult and requires a much more elaborate scheme than in the CT case. This shall be subject to future investigations. Since the boundaries of the pelvic bone are much easier to detect in CT data the current experiments serve as a preliminary study to test the performance of the statistical shape model itself (section 4).

Further author information: (Send correspondence to H. Lamecker)

H.Lamecker: E-mail: lamecker@zib.de, Telephone: +49 30 84185 177

M. Seebaß: E-mail: seebass@indeed3d.com, Telephone: +49 30 84185 328

H.-C. Hege: E-mail: hege@zib.de, Telephone: +49 30 84185 141

P. Deuffhard: E-mail: deuffhard@zib.de, Telephone: +49 30 84185 101

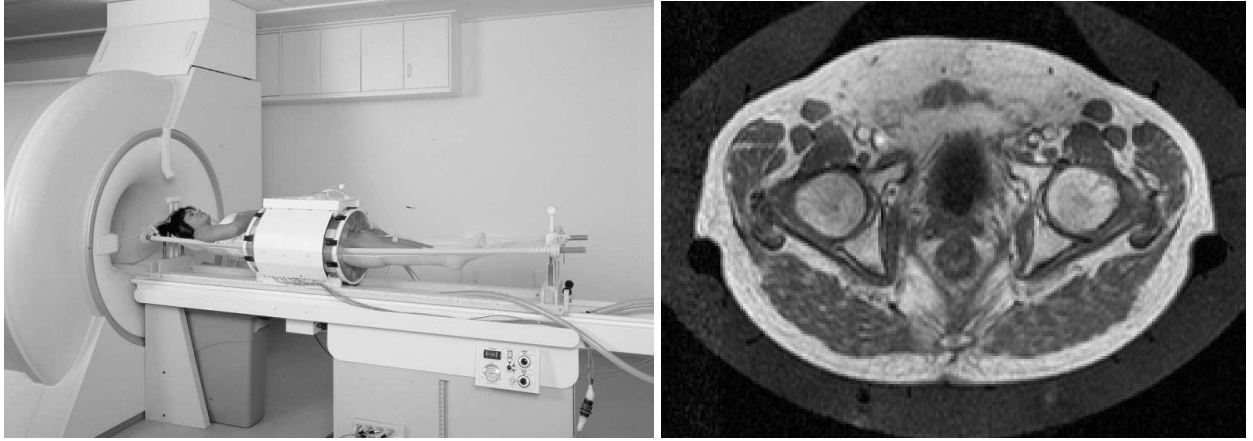


Figure 1. Left: hybrid system (MRT plus applicator), Right: MRT slice image from the abdomen with pelvic bone.

1.2. Previous work

Generating statistical shape models is a challenging task especially for shapes of complicated topology like the pelvic bone (genus 3). The main problem is the need to establish correspondences between different shapes in the training set, i.e. to match anatomically equivalent features. This becomes particularly difficult in 3D. Several approaches for defining good correspondences have been proposed:

A method for 3D shape correspondence using local geometry and geodesics is described by Wang et al.¹ without its application to statistical shape models. It is evaluated by computing residual surface distances. Kelemen et al.² represent the shapes by their expansion into a series of elliptical harmonics. The PCA is performed on the parametric description in contrast to the point distribution model used by Cootes et al.³ Thompson et al.⁴ compute a mapping from each shape onto a sphere using a deformable model approach. Correspondence between two spheres, constrained by matched anatomical feature lines, is established by means of a warping algorithm. Only shapes with sphere-like topology can be treated in the previous two approaches. Fleute et al.⁵ establish correspondence by elastic registration of a template shape with all other shapes based on minimizing Euclidean distance. Closely related is the approach of Frangi et al.⁶ The PCA is performed on the points of the control grids computed from an elastic registration on binary volumetric data. Brett et al.^{7,8} present two approaches of automatic construction of shape models based on polyhedral shape representation. One minimizes the Euclidean distance between shapes on different levels of detail, obtained by triangle decimation. The related problem of surface folding is relaxed by their second approach of parameterizing surfaces onto common planar domains using harmonic maps. Their method applies only to surfaces homeomorphic to discs and does not guarantee fold-over free mappings however (see⁹ for an illustration of this fact). Davies et al.¹⁰ define the correspondences using an information theoretic minimal description length approach. Here the optimality criterion is the compactness of the model. The optimization of this criterion is very expensive. The method has been applied to 2D-examples and an extension to 3D shapes with sphere-like topology is outlined.

The method used in this work has been described by Lamecker et al.^{11,12} for the construction of a statistical shape model of the liver. It is based on the idea on minimizing metric distortion and consistent patch-wise parameterization of the shapes. It is interactive, yet able to handle shapes of arbitrary topology.

2. TRAINING PHASE

2.1. Statistical Shape Models

A statistical model is built from a training set of shapes \mathbf{v}_i ($i = 1, \dots, N$). Each shape \mathbf{v}_i is given by M points sampled on its surface (thus $\mathbf{v}_i \in \mathbb{R}^{3M}$). Using principal component analysis each shape vector can be expressed

using a linear model of the form

$$\mathbf{v}_i = \bar{\mathbf{v}} + \mathbf{P}\mathbf{b}_i = \bar{\mathbf{v}} + \sum_k \mathbf{p}^k b_i^k \quad (1)$$

where $\bar{\mathbf{v}}$ is the mean shape vector and $\mathbf{P} = \{\mathbf{p}^k\}$ the matrix of eigenvectors of the covariance matrix. The corresponding eigenvalues $\{\lambda^k\}$ describe the amount of variance in the direction of the eigenvectors. The shape parameters $\mathbf{b} = \{b^k\}$ control the modes of variation.

In order to obtain a correct statistical model all M points on each surface (a) must correspond in an anatomical meaningful way, *and* (b) their coordinates must be given relative to a common frame of reference (alignment). This is crucial, since incorrect correspondences can either introduce too much variation or lead to illegal instances of the model.

Note that - in general - these two goals can be accomplished independently of one another. Often, however, an initial alignment precedes the computation of corresponding points (e.g. when corresponding points are supposed to be closest points). In this work we will employ a method, that does *not* rely on an initial alignment (see section 2.2). Once correspondence has been established, the alignment will be computed in the following way:

Without loss of generality, let \mathbf{v}_1 define the reference coordinate system, which all other shapes \mathbf{v}'_j ($j > 1$) will be aligned to. Let $\mathbf{x}_{1,k}$ denote the coordinates of the shape vector \mathbf{v}_1 , and $\mathbf{x}'_{j,k}$ the coordinates of \mathbf{v}'_j respectively. Then we compute a rigid transformation $\mathbf{T}_{j,\min}$ that minimizes the sum of squared distances between corresponding pairs $\mathbf{x}_{1,k}$ and $\mathbf{x}'_{j,k}$ ($k = 1, \dots, M$), for all $j > 1$:

$$\mathbf{T}_{j,\min} = \arg \min_{\mathbf{T}} \sum_{k=1}^M \|\mathbf{x}_{1,k} - \mathbf{T}\mathbf{x}'_{j,k}\|^2$$

This minimization problem can be solved by singular value decomposition.¹³ The coordinates of the final shape vector \mathbf{v}_j will then be $\mathbf{x}_{j,k} = \mathbf{T}_{j,\min}\mathbf{x}'_{j,k}$.

This procedure introduces some bias towards the reference system \mathbf{v}_1 , which can be reduced by iterative refinement (see e.g. Frangi et al.⁶). However we have seen in our experiments that the influence of this defect is rather small.

2.2. Solving the correspondence problem

Establishing correspondence between two topologically equivalent 3D shapes $\mathcal{S}_1, \mathcal{S}_2$, represented as triangular meshes, means computing a homeomorphic mapping

$$f : \mathcal{S}_1 \rightarrow \mathcal{S}_2 ,$$

possibly under additional constraints (e.g. specifically given correspondences of points or lines of anatomical or geometrical significance). Depending on these constraints, there may be many solutions to this problem. Hence there is a need to impose further restrictions, that define optimal correspondences.

Since we are dealing with anatomical shapes, we propose that f is required to introduce as little distortion as possible, i.e. preserve the metric structure of \mathcal{S}_1 by approximately keeping angles fixed and allowing for a global scaling of \mathcal{S}_1 .

In this work we will present an approximate solution to this problem. f will be computed by mapping both shapes \mathcal{S}_1 and \mathcal{S}_2 to a common base domain D homeomorphic to \mathcal{S}_1 or \mathcal{S}_2 . Hence we are left with the problem of finding a mapping $f_i : \mathcal{S}_i \rightarrow D$ for each shape i , meeting the requirements defined above.

$$\begin{array}{ccc} \mathcal{S}_1 & \xrightarrow{f_2^{-1} \circ f_1} & \mathcal{S}_2 \\ & \searrow f_1 & \swarrow f_2 \\ & & D \end{array} \quad (2)$$

The method will be explained in more detail in the remainder of this section.

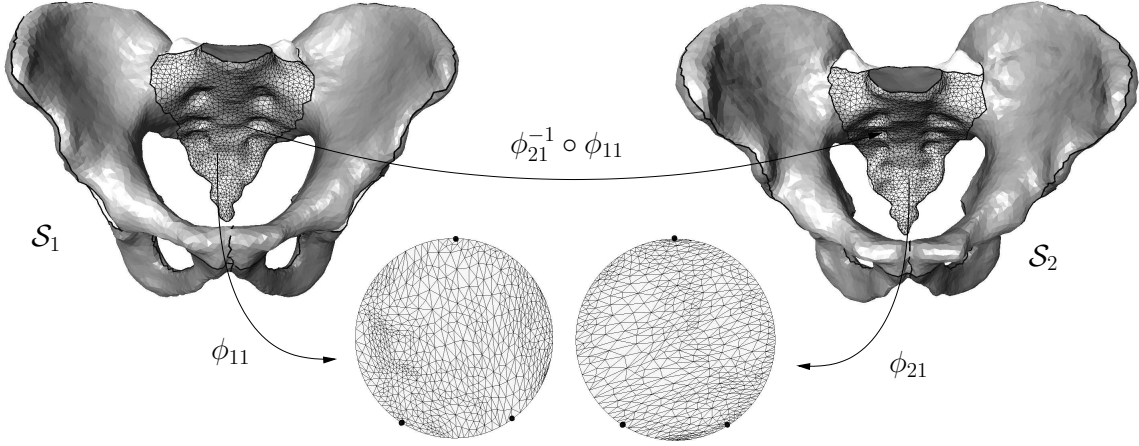


Figure 2. A homeomorphism f between the shapes \mathcal{S}_1 and \mathcal{S}_2 is computed by mapping each patch of the two shapes onto a disc using the shape preserving mappings ϕ_{11} and ϕ_{21} respectively. The boundaries are mapped to the unit circle by fixing all branching points according to their average arc-length on both surfaces to be matched. All edges on the boundaries are mapped according to their arc-length on the original surfaces. The resulting mapping for one patch is given by $\phi_{21}^{-1} \circ \phi_{11}$.

Surfaces homeomorphic to discs. Let us consider the easiest case, where \mathcal{S}_1 and D are homeomorphic to a disc. Moreover let $D \subset \mathbb{R}^2$ be a convex region. As an additional constraint, we require the boundary of \mathcal{S}_1 to be mapped smoothly to the boundary of D .

We use *convex-combination maps*¹⁴ to flatten \mathcal{S}_1 to D . Without loss of generality, let

$$X = \{\mathbf{x}_1, \dots, \mathbf{x}_n, \mathbf{x}_{n+1}, \dots, \mathbf{x}_N\} \quad (3)$$

be the coordinates of the vertices of the surface triangulation \mathcal{S}_1 . Assume that $\mathbf{x}_1, \dots, \mathbf{x}_n$ are internal nodes, while $\mathbf{x}_{n+1}, \dots, \mathbf{x}_N$ lie on the boundary. Furthermore let $\mathbf{u}_i \in D \subset \mathbb{R}^2$ ($i = 1, \dots, N$) be the corresponding coordinates in the parameter domain. The mapping

$$\phi : X \rightarrow D, \quad \mathbf{x}_i \mapsto \mathbf{u}_i = \phi(\mathbf{x}_i)$$

is called a *convex combination map*, if

$$\mathbf{u}_i = \sum_{j=1}^N \lambda_{ij} \mathbf{u}_j \quad (4)$$

for all internal nodes $i = 1, \dots, n$, and

$$\sum_{j=1}^N \lambda_{ij} = 1 \quad , \quad \lambda_{ij} \begin{cases} = 0 & (i, j) \notin E \\ > 0 & (i, j) \in E \end{cases} \quad (5)$$

where E is the set of all edges of the triangulation. It was shown by Floater¹⁴ that ϕ does not produce any fold-overs in the planar triangulation, and every node \mathbf{u}_i lies in the convex hull of ∂D . Computing ϕ amounts to solving the linear system (4) under the constraints of (5). Floater also showed that there exists a unique solution to this problem. Since (4) is a sparse linear system of equations, it can be solved efficiently.

The question remains on how to choose the convex combination weights λ_{ij} . We are interested in producing a mapping, that preserves the metric structure of the surface \mathcal{S}_1 as good as possible. We use here the idea of locally approximating the *geodesic polar map*,¹⁵ first presented by Floater.¹⁴ Thereby λ_{ij} are computed as convex weights in the planar domain, such that the angles and lengths of the original triangulation are preserved as good as possible. The resulting map is called *shape preserving map*. Please refer to Floater¹⁴ for details.

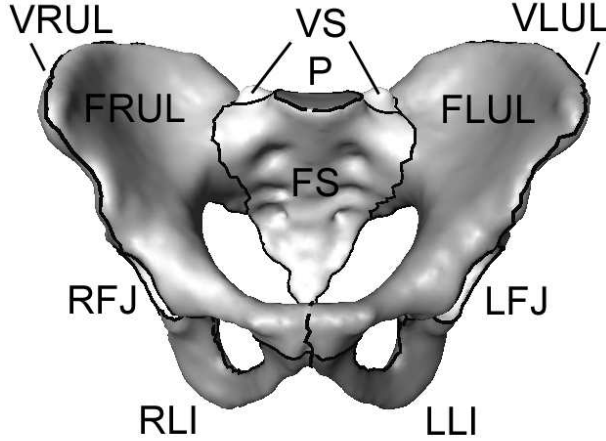


Figure 3. Pelvic bone decomposition.

Arbitrary surfaces. For establishing correspondence between two arbitrary surfaces we employ the method of consistent surface parameterization as presented by Zöckler et al.¹⁶ An arbitrary surface is thereby divided into n_p patches, each homeomorphic to a disc. This decomposition needs not only to be topologically equivalent on all surfaces of the training set but also to represent similar anatomical regions in order to get a meaningful correspondence. Each corresponding pair of patches is mapped onto a common planar convex base domain via ϕ_{ij} , where $i = 1, 2$ represents the shape and $j = 1, \dots, n_p$ enumerates the patches. We choose the unit disc (radius 1, centered at the origin) as the base domain. Continuous continuation over ϕ_{ij} , $j = 1, \dots, n_p$ results in the full mapping $f_i : S_i \rightarrow D$, where in this case D represents a set of unit discs. To achieve continuity across patch borders the patch boundaries are mapped to the unit circle according to their average arc-length on the two surfaces to be matched (see figure 2). Branching points (vertices, that belong to more than one boundary) are thus fixed on the circle, while all boundary edges are mapped according to the arc-length on their original surface.

The patch decomposition is an interactive process. The patch boundaries are drawn on the surface by manually selecting points where two or more patch boundaries would meet (branching points). Some intermediate points along the patch boundaries may be added manually. These points are then automatically connected by computing geodesic shortest paths between them. In almost all cases we use a metric that favors paths along lines of high curvature, when these lines represent anatomical features. In other cases we use a pure distance measure. Note that since the definition of the patch boundaries is independent of the location and orientation of the surface in space, the whole process of establishing correspondences does not rely on any initial alignment of the surfaces.

2.3. Pelvic Bone model

We have generated a statistical shape model of the *pelvic bone* from 23 CT data sets of male patients. Each data set was manually segmented by labeling the pelvic bone regions. Before surface reconstruction a label based interpolation algorithm is applied to reduce the effect of anisotropy of the voxels (slice thickness of 5 mm, resolution of 1.4 mm in axial slices). For reasons of efficiency all surfaces are simplified¹⁷ by reducing the number of triangles, obtaining meshes with about 25000 triangles and 12500 nodes. Each pelvic bone surface was divided into 11 patches (figure 3):

- the promontorium (P)
- the frontal/ventral sacrum (FS, VS)
- the frontal right/left upper ilium (FRUL, FLUL)

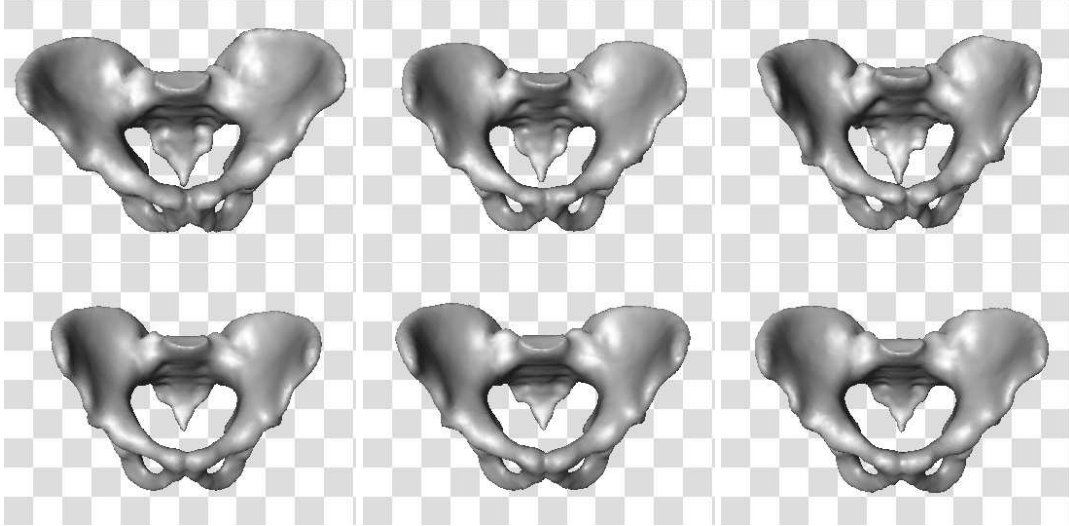


Figure 4. Variability of a statistical model of the pelvic bone shape made from 23 training data sets: in the left column the eigenmode with the largest variance λ_1 is varied between $\pm 3\sqrt{\lambda_1}$, in the second and third column the modes with the second and third largest variance are shown respectively.

- the ventral right/left upper ilium (VRUL, VLUL)
- the right/left femur joint (RFJ, LFJ)
- the right/left lower ilium (RLI, LLI)

Following the procedure described in section 2.2 the user had to specify about 40 landmarks per surface, resulting in 11 patches, divided by 40 patch boundaries and 25 branching points. Manual interaction amounts to about 30 minutes per training data.

The main modes of variation of the pelvic bone (see figure 4) model can be well interpreted as: (1) scaling in z-direction, (2) widening and bending of the ilium and (3) change of length of the sacrum.

3. SEGMENTATION PHASE

3.1. Segmentation Strategy

The segmentation strategy based on our statistical shape model does not essentially differ from the one used by Cootes et al.³ apart from the fact that we use a different iteration scheme. The core adjustment procedure of the segmentation strategy consists of two steps:

- First a displacement vector $\Delta \mathbf{x}_i$ for each point \mathbf{x}_i on the model surface is computed from an analysis of the grey value profile along the surface normal. Cootes et al.³ compute $\Delta \mathbf{x}_i$ by statistically modeling the profiles in the training set and matching the current profile to this model. We will use a fixed model to compute $\Delta \mathbf{x}_i$, that will be explained in detail in section 3.2.
- Next a weighted least squares approximation between the shape model $\mathcal{S}(\mathbf{b}, T) = T(\bar{\mathbf{v}} + P\mathbf{b})$ and the displaced surface points $\mathbf{x}_i + \Delta \mathbf{x}_i$ is computed. The approximation is either performed with respect to the position parameters T (position adjustment) or with respect to the shape parameters \mathbf{b} (shape adjustment). To prevent extreme shapes the allowed range for the shape parameters is restricted to the minimal and maximal values as derived from the training data.

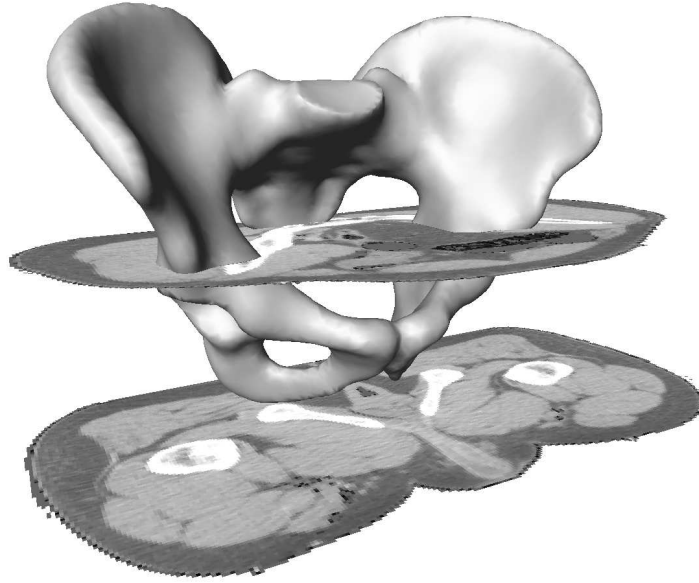


Figure 5. Initialization of model-based segmentation

The segmentation process is initialized by positioning the mean shape \bar{v} into the image data manually. At each iteration of the segmentation process, several position adjustments are performed until no further significant improvement is achieved. Then a single shape adjustment is applied. This process is repeated until convergence. To improve the robustness a multilevel strategy has been implemented where the number of shape modes in the weighted least squares approximation is increased successively. At the first level only the three most important modes are fitted to the data. For each subsequent level three more modes are added until the maximum number of modes is reached.

3.2. Grey-value Profile Analysis

To test the capability of the pelvic bone model for segmentation we performed experiments on CT data. We will therefore describe a method for the computation of displacements Δx_i from CT data.

The profiles are sampled from the data by tri-linear interpolation. Their length is 25 mm in both directions (inside/outside), 50 points are taken. In CT data bone is rather well distinguishable from surrounding tissues by its large intensity. The analysis therefore consists of scanning each profile from the outside towards the inside. Whenever the intensity I rises below a certain threshold at point x we take $\Delta x_i = x - x_i$. We chose a threshold of 120 Hounsfield Units (HU).

In cases where the profile intersects the surface more than once or leaves the bounding box of the CT data, the profile will be restricted to a suitable length. If a surface point does not lie inside the bounding box of the CT at all, this point is assigned weight 0 in the weighted least squares approximation. These cases are checked at each adjustment step of the segmentation process.

4. RESULTS

We will focus our experiments around the following questions:

- How *complete* is our model, i.e. how well does it describe arbitrary shapes that are not explicitly incorporated into the model?
- Is our grey value profile model well suited?
- Using the shape and the profile model, which accuracy can be achieved when segmenting CT data sets, that are not contained in the model?

For the experiments conducted below, all data from the model building process were considered. Hence all experiments were performed on a pool of 23 data sets, where the manual segmentations are referred to as the gold-standard (they will be called reference surfaces).

4.1. Evaluation measures

In order to quantify the segmentation accuracy, suitable measures for comparing 3D shapes have to be devised. In this section we give precise definitions for evaluation criteria, that we believe are useful and intuitive for evaluation purposes.

Given two surfaces \mathcal{S} and \mathcal{S}' we define the distance $d(\mathbf{x}, \mathcal{S}')$ between a point \mathbf{x} on a surface \mathcal{S} and the surface \mathcal{S}' as:

$$d(\mathbf{x}, \mathcal{S}') = \min_{\mathbf{x}' \in \mathcal{S}'} \|\mathbf{x} - \mathbf{x}'\|_2 \quad (6)$$

where $\|\cdot\|_2$ denotes the Euclidean norm. The following distance measures are chosen to be symmetric when exchanging \mathcal{S} with \mathcal{S}' in order not to lose important information. Let $|\mathcal{S}|$ denote the area of the surface.

Mean Distance:

$$d_{\text{mean}}(\mathcal{S}, \mathcal{S}') = \frac{1}{|\mathcal{S}| + |\mathcal{S}'|} \left(\int_{\mathbf{x} \in \mathcal{S}} d(\mathbf{x}, \mathcal{S}') d\mathcal{S} + \int_{\mathbf{x} \in \mathcal{S}'} d(\mathbf{x}, \mathcal{S}) d\mathcal{S} \right) \quad (7)$$

Root Mean Square Distance:

$$d_{\text{rms}}(\mathcal{S}, \mathcal{S}') = \sqrt{\frac{1}{|\mathcal{S}| + |\mathcal{S}'|} \left(\int_{\mathbf{x} \in \mathcal{S}} d(\mathbf{x}, \mathcal{S}')^2 d\mathcal{S} + \int_{\mathbf{x} \in \mathcal{S}'} d(\mathbf{x}, \mathcal{S})^2 d\mathcal{S} \right)} \quad (8)$$

Maximum/Hausdorff distance:

$$d_{\text{max}}(\mathcal{S}, \mathcal{S}') = \max \left(\max_{\mathbf{x} \in \mathcal{S}} d(\mathbf{x}, \mathcal{S}'), \max_{\mathbf{x} \in \mathcal{S}'} d(\mathbf{x}, \mathcal{S}) \right) \quad (9)$$

Area of deviation: The idea is to have a measure that is not as local as the Hausdorff distance and not as global as the mean distance and allows intuitive imagination of shape difference. The relative surface area on which the deviations are larger than some threshold t presents such a compromise:

$$d_r(\mathcal{S}, \mathcal{S}', t) = \frac{1}{|\mathcal{S}| + |\mathcal{S}'|} \cdot \left(\int_{\mathbf{x} \in \mathcal{S}} \Theta(d(\mathbf{x}, \mathcal{S}') - t) d\mathcal{S} + \int_{\mathbf{x} \in \mathcal{S}'} \Theta(d(\mathbf{x}, \mathcal{S}) - t) d\mathcal{S} \right) \quad (10)$$

where Θ is the Heaviside-Theta function.

4.2. Completeness

The completeness of a statistical model is its generalization ability or its ability to describe shapes that have not been incorporated in the training set. We test the completeness of our model in a leave-one-out test: for each of our 23 pelvic bone shapes, we match a model built from all other 22 shapes to the particular pelvic bone shape. This is achieved by minimizing the symmetric RMS distance (8) between the model \mathcal{S} and the reference surface \mathcal{S}' over the shape parameters $\mathbf{b} = \{b^k\}$ and the transformation parameters of a rigid transformation \mathbf{T} :

$$\min_{\mathbf{b}, \mathbf{T}} \{d_{\text{RMS}}(\mathcal{S}(\mathbf{b}, \mathbf{T}), \mathcal{S}')\} \quad (11)$$

We use a quasi-Newton optimization scheme to compute \mathbf{b}, \mathbf{T} . On average the shapes can be represented with a mean distance error of 1.6 ± 0.2 mm (see row 2 of Table 1).

4.3. Leave-all-in Segmentation

For analyzing the performance of our grey value profile model, we segment all training data with a shape model that incorporates all training shapes. Therefore we expect the results only to depend on the profile modeling and the overall segmentation strategy, but not the statistical shape model itself, since all shapes are represented in the model. On average the mean distance of the segmented surface to the reference surface is 0.6 ± 0.2 mm. The average surface area with deviations larger than 3 mm is 1.3 ± 1.6 % (see row 1 of Table 1).

	d_{mean} [mm]	d_{RMS} [mm]	d_{max} [mm]	$d_r(3\text{ mm})$ [%]
leave-all-in segmentation (23)	0.6 ± 0.2	0.8 ± 0.3	4.7 ± 1.6	1.3 ± 1.6
shape model optimization (22)	1.6 ± 0.2	2.2 ± 0.2	14.6 ± 3.8	15.8 ± 5.4
leave-one-out segmentation (22)	1.8 ± 0.2	2.4 ± 0.3	15.6 ± 4.2	18.3 ± 4.3

Table 1. Results of the leave-all-in segmentation (row 1: initialization by starting from optimal guess), the leave-one-out shape model optimization (row 2) and the leave-one-out segmentation (row 3). The number in brackets indicates how many training shapes are incorporated in the particular model. 23 data sets were segmented automatically. The different error measures are defined in the text in section 4.1.

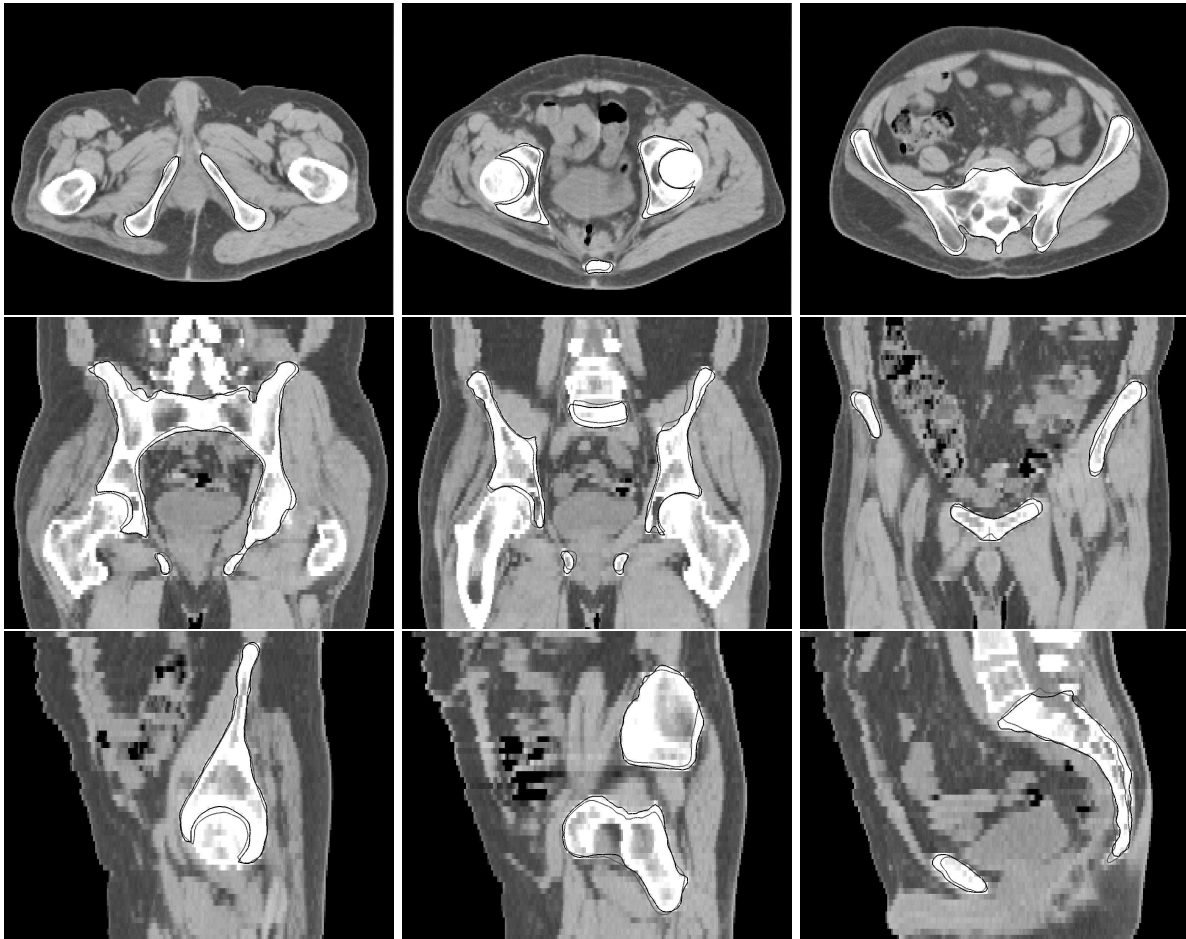


Figure 6. Example of a leave-one-out (grey contours) versus the leave-all-in (black line) segmentation result. Three axial, three coronal and three sagittal slices with intersection lines of the 3D surfaces are shown. The mean surface distance errors of the leave-one-out and the leave-all-in segmentation are 1.7 mm and 0.4 mm, respectively. The deviation is larger than 3 mm on 17.0% and 0.2% of the surface area, respectively.

4.4. Leave-one-out Segmentation

We are now interested to see how the actual segmentation on arbitrary CT data sets performs. We carried out a leave-one-out test on all 23 data sets each time segmenting it with a model made from the other 22 shapes. The average mean surface distance is 1.8 ± 0.2 mm and the average surface area with deviations larger than 3 mm is 18.3 ± 4.3 % (see row 3 of Table 1).

5. DISCUSSION AND CONCLUSIONS

In this work we demonstrate how to generate a statistical model of the pelvic bone shape. The algorithm for solving the correspondence problem is efficient even for the complicated topology of the pelvic bone. We show that the principal modes of variation are well interpretable and that the model is well suited for the purpose of segmentation. This is quantitatively undermined in a study of segmenting 23 CT data sets from different male patients. Although the accuracy of the leave-all-in experiment is satisfactory (mean surface distance of 0.6 mm), the leave-one-out experiment yields insufficient results (mean surface distance of 1.8 mm). From the shape optimization (mean surface distance of 1.6 mm) however we can conclude that the leave-one-out segmentation is close to optimal in the sense that the results do not depend on the segmentation strategy but only on the variance captured by the training set. Consequently the size of the training set needs to be enlarged in order to obtain better results.

The modes of the statistical shape model are well interpretable due to the fact that a large set of anatomical features are matched throughout the training set by the definition of the patch decomposition. However, the objective of minimizing local distortion of the surfaces is only approximatively met by our method. Large distortions especially occur along the patch boundaries. As an improvement we intend to relax the surface triangulation after the initial parameterization by moving the triangle nodes on the surface, constraining only those nodes that represent distinct features (landmarks, nodes along lines of high curvature, etc.). During the segmentation process lateral displacements are not desirable, since they do not modify the shape. Hence a second relaxation process at each adjustment step of the algorithm might further improve the results.

The main goal for the future is to establish a gray value profile model for the segmentation of MRT data. It remains to be seen whether an explicit scheme can be successful or statistical modeling of the grey values will be preferable.

The results of the experiments conducted in this work suggest that using an enlarged statistical shape model is a promising approach for MRT segmentation.

ACKNOWLEDGMENTS

This work was supported by the DFG Research Center "Mathematics for key technologies" (FZT 86) in Berlin. The authors thank Thomas Lange for his contribution in establishing the evaluation process for the segmentation experiments, as well as Johanna Gellermann and Peter Wust for providing the medical image data.

REFERENCES

1. Y. Wang, B. S. Peterson, and L. H. Staib, "Shape-based 3D surface correspondence using geodesics and local geometry," in *CVPR 2000*, **2**, pp. 644–651, 2000.
2. A. Kelemen, G. Székely, and G. Gerig, "Three-dimensional model-based segmentation of brain MRI," *IEEE Trans. on Medical Imaging* **18**(10), pp. 828–839, 1999.
3. T. Cootes, A. Hill, C. J. Taylor, and J. Haslam, "Use of active shape models for locating structures in medical images," *Image and Vision Computing* **12**, pp. 355–366, 1994.
4. P. M. Thompson and A. W. Toga, "Detection, visualization and animation of abnormal anatomic structure with a deformable probabilistic brain atlas based on random vector field transformations," *Medical Image Analysis* **1**(4), pp. 271–294, 1996.
5. M. Fleute, S. Lavalée, and R. Julliard, "Incorporating a statistically based shape model into a system for computed-assisted anterior cruciate ligament surgery," *Medical Image Analysis* **3**(3), pp. 209–222, 1999.
6. A. F. Frangi, D. Rückert, J. A. Schnabel, and W. J. Niessen, "Construction of multiple-object three-dimensional statistical shape models: Application to cardiac modelling," *IEEE Transactions on Medical Imaging* **21**(9), pp. 1151–1166, 2002.
7. A. D. Brett and C. J. Taylor, "A method of automated landmark generation for automated 3D PDM construction," *Imag. Vis. Comp.* **18**(9), pp. 739–748, 2000.
8. A. D. Brett and C. J. Taylor, "Automated construction of 3D shape models using harmonic maps," in *Medical Image Understanding and Analysis*, S. Arridge and A. Todd-Pokropek, eds., pp. 175–178, (London, U.K.), 2000.

9. T. Duchamp, A. Certain, T. DeRose, and W. Stuetzle, "Hierarchical computation of PL harmonic embeddings," tech. rep., University of Washington, July 1997.
10. R. H. Davies, C. Twining, T. Cootes, J. C. Waterton, and C. J. Taylor, "A minimum description length approach to statistical shape modelling," *IEEE Transactions on Medical Imaging* **21**, pp. 525–537, May 2002.
11. H. Lamecker, T. Lange, and M. Seebaß, "A statistical shape model for the liver," in *MICCAI 2002*, **2489**, pp. 422–427, 2002.
12. H. Lamecker, T. Lange, and M. Seebaß, "Segmentation of the liver using a 3d statistical shape model," *submitted*, 2003.
13. A. D. McLachlan, "Least squares fitting of two structures," *J. Mol. Biol.* **128**, pp. 74–79, 1979.
14. M. S. Floater, "Parameterization and smooth approximation of surface triangulations," *Computer Aided Geometric Design* **14**(3), pp. 231–250, 1997.
15. B. O'NEILL, *Elementary differential geometry*, Academic press, 1966.
16. M. Zöckler, D. Stalling, and H.-C. Hege, "Fast and intuitive generation of geometric shape transitions," *The Visual Computer* **16**(5), pp. 241–253, 2000.
17. M. Garland and P. S. Heckbert, "Simplification using quadratic error metrics," in *SIGGRAPH 97*, pp. 209–216, 1997.